DOI: 10.1021/ma100285v

Macromolecules
ARTICLE

Thermoreversible Micelle Formation Using a Three-Armed Star Elastin-like Polypeptide

Ali Ghoorchian, James T. Cole, and Nolan B. Holland*

Department of Chemical & Biomedical Engineering, Cleveland State University, 2121 Euclid Avenue, Cleveland, Ohio 44115

Received February 4, 2010; Revised Manuscript Received March 31, 2010

ABSTRACT: We have designed, synthesized, and purified a novel three-armed star polymer consisting of an elastin-like polypeptide (ELP) followed by a negatively charged trimer-forming oligomerization domain at the C-terminus. In low salt conditions, the water-soluble trimers assemble into micellar particles as small as 25 nm in diameter when heated to temperatures above their transition temperature. The size of these micelles can be controlled by adjusting salt and cosurfactant concentrations. They are stable at elevated temperatures but will dissociate into the individual trimers when the temperature is again decreased below the transition temperature. Their behavior at high temperatures is quite different than typical ELP constructs, which initially form large aggregates followed by phase separation into a coacervate and soluble fraction. The polypeptide consists of 40 pentapeptide repeats of glycine−valine−glycine−valine−proline (GVGVP) followed by the 27 amino acid foldon domain. It is expressed in *E. coli* and purified by thermal transition cycling.

Introduction

Elastin-like polypeptides (ELP) are a part of the family of responsive polymers that have been studied extensively for the past two decades.[1−3] These polymers consist of repeats of the sequence GαGβP, where α can be any of the 20 naturally occurring amino acids and β can be any except for proline.[1] These polypeptides are similar to responsive synthetic polymers like PNIPAA in many ways. This includes the fact that both exhibit LCST (lower critical solution temperature) behavior by phase separating above a specific transition temperature.[1,4] When these materials are prepared as bulk hydrogels, this behavior results in significant volume changes when passing through the transition temperature. These so-called responsive materials have been used for many different applications including drug delivery,[5,6] tissue engineering,[7,8] surface engineering,[9−11] nanosensors,[12] and hydrogels.[1,13,14] The environmental stimuli for both synthetic polymers and elastin-like polypeptides can be chosen based on the intended application and can include temperature,[1,2] pH,[15,16] ionic strength,[16] or light.[17,18]

An area that elastin-like polypeptides have attracted much attention is the molecular self-assembly of ELP constructs into nano- and microscale constructs.[19−23] Several different block copolymers (either AB or ABA) consisting of ELP chains with different hydrophobicities have been designed.[5,24] These constructs assemble into particles when triggered by external stimuli that cause one of the ELP chains of the copolymer to become hydrophobic, leaving the second soluble ELP block to act as a hydrophilic headgroup that stabilizes the formation of micellar or vesicular particles.

Drug delivery using self-assembled particles[25,26] is an attractive area for ELP because of the ability to precisely control the structure of these polypeptides[27] and their natural biocompatibility.[28] ELP constructs have demonstrated efficacy in properties desirable for drug delivery carriers including targeted delivery,[29] good loading capacity,[30] and low clearance in animals.[31] The most important environmental stimuli for a drug delivery carrier are the ones which have physiological relevance, i.e., pH difference between the healthy and diseased cells, temperature, concentration difference, or a combination of these[32,33] and ELP molecules have the capacity to be designed and constructed to respond to any of these environmental stimuli. Another advantage of ELP self-assembled particles is their small size. These particles can be 100 nm or less, which is much smaller than typical ELP aggregates. The smaller size can be an advantage *in vivo* by decreasing antigenicity and reducing clearance.[24]

Although the specifics of ELP aggregation at the molecular level are still debated, an early description of the process suggested that the ELP chains transition from a random coil conformation to a folded β-spiral which is hydrophobic.[1,34] The folded polypeptides are partially stabilized by forming a twisted filament of three chains and phase separating in the form of a coacervate.[35] This process results in the measurable turbidity of the solution above its transition temperature. This theory has been supported by a number of studies, especially by using circular dichroism (CD) measurements.[2,36] In a recent report, it was demonstrated that combining ELP with the trimer forming α-helical coiled coil motif resulted in the tail ends of the ELP coming into close proximity above the transition temperature, further supporting this model.[37]

There are numerous protein folds that incorporate such a triple helix, including the collagen triple helix and the α-helical coiled coil motif. Another instance is in bacteriophage T4 fibritin protein, which forms a fibrous trimer. Unlike the collagen and α-helical coiled coil, the fibritin fold is not stable alone but requires a terminal trimer folding domain to stabilize it.[38] This domain, called foldon, can be expressed as a 27 amino acid peptide which forms a homotrimer in a large range of pH, with the notable exception of very low pH.[39,40] At neutral pH, the domain is negatively charged and thermally stable up to 75 °C.[38] These features have been used to stabilize short triple helices of

*Corresponding author: phone (216) 687-2572; e-mail n.holland1@csuohio.edu.

 Published on Web 04/16/2010

collagen for structural studies using recombinant methods to incorporate foldon.[41] With the 27 amino acid sequence at either the N- or C-terminus, a collagen triple helix can be stabilized at higher temperatures and lower concentrations than one without the foldon sequence.[38]

We report here the design and biosynthesis of a new elastin-like polypeptide construct that incorporates the foldon domain at its C-terminal end. We demonstrate that the foldon domain folds, producing a trimer resulting in a three-armed star ELP. The thermal transitions of this construct are compared to linear ELP at different polypeptide and salt concentrations. Additionally, we show that this construct behaves quite differently at low salt concentrations by forming nanoscale micellar aggregates at temperatures above the ELP transition temperature. We describe generally the conditions that lead to the formation of these micelles.

Materials and Methods

Gene Design and Preparation. The synthesis of the elastin-like polypeptide gene was based on the methods described by Meyer and Chilkoti.[27] In short, complementary oligonucleotides (Invitrogen) encoding five repeats of amino acid sequence GVGVP were designed to have appropriate overhangs to insert into pUC19 cloning vector (Novagen) digested with *Eco*RI and *Hin*DIII as well as internal cut sites for restriction enzymes *Bgl*I and *Pfl*MI. These two oligonucleotides were annealed together by heating to 95 °C and slowly cooling in a thermocycler. An aliquot of pUC19 vector was double digested using *Eco*RI and *Hin*DIII and then purified using a DNA extraction kit (GenScript). The annealed DNA was ligated into the double digested vector in a 3 to 1 molar ratio using Quick Ligase (New England Biolabs) for 15 min. A 10 μL aliquot of the ligation product was combined with 50 μL of chemically competent *E. coli* cells and transformed by heat shocking (30 min at 4 °C followed by 2 min at 37 °C) and left overnight on solid agar plates supplemented by 100 mg/L of ampicillin. Colonies were grown overnight and screened by using PCR screening techniques. The sequence was ultimately confirmed by DNA sequencing.

To increase the length of the ELP encoding DNA, we double digested the pUC19 vector containing $(GVGVP)_5$ with *Nde*I and *Pfl*MI restriction enzymes. A separate sample of the same plasmid was also double digested by using *Nde*I and *Bgl*I restriction enzymes to produce the insert. Using double digestions minimizes the number of false positives on the plates after transformation and does not require dephosphorylation of the vectors. This process resulted in DNA encoding 10 GVGVP repeats. This process was repeated twice more to reach $(GVGVP)_{40}$. This $(GVGVP)_{40}$ encoding DNA was transferred to a pET20b expression vector modified as described by Meyer and Chilkoti[27] to have one *Sfi*I recognition site that leaves an overhang that is compatible with the *Pfl*MI cutsite in the pUC19 construct. The $(GVGVP)_{40}$ DNA resulting from the digestion of the pUC vector with *Nde*I and *Pfl*MI was inserted into the pET vector digested with *Nde*I and *Sfi*I. The resulting gene encodes a 206 amino acid polypeptide: $MGH(GVGVP)_{40}GWP$.

To prepare DNA encoding the foldon domain, oligonucleotides were designed so they would anneal into a double-stranded DNA cassette with overhangs compatible with the *Sfi*I cut site, leaving a *Pfl*MI recognition site. The codons were selected for optimal expression in *E. coli*.[42] This construct was ligated into the modified pET20b vector described above digested with *Sfi*I. A $(GVGVP)_{40}$ encoding DNA was then inserted as above resulting in the 233 amino acid polypeptide that includes a C-terminal foldon domain sequence: $MGH(GVGVP)_{40}GWP$-GYIPEAPRDGQAYVRKDGEWVLLCTFL.

Protein Expression and Purification. Expressions were started by preparing a 5 mL overnight starter culture from frozen stock in LB medium supplemented with 100 μg/mL ampicillin (LBA) at 37 °C. The starter culture was added to 1 L of LBA medium in a 2 L Erlenmeyer flask and shaken at 300 rpm and 37 °C to an OD_{600} of between 0.9 and 1.0, at which point expression was induced by adding 0.1 mM IPTG. The cells were harvested after 4−5 h by centrifugation for 30 min at 3000*g*. To lyse the cells, they were resuspended in 20 mL of bacterial protein extraction reagent (B-PER, Pierce) by vortexing vigorously for several minutes. The lysed cells were then centrifuged at 4 °C for 20 min at 20 000*g* to separate the soluble protein from insoluble cell lysate. The soluble supernatant, which contained our polypeptide, was then purified using inverse transition cycling method.[43] We utilized warm centrifugation of the protein solution for 15 min at about 40 °C at 15 000*g* to pellet out the aggregated proteins. The isolated pellet was resuspended by using 5 mL of chilled PBS buffer pH 7.4 (Fisher Scientific). The resuspended solution was then centrifuged at 4 °C for 15 min at 15 000*g*. This process was repeated two times to purify the ELP.

Protein Characterization. Purified ELP was characterized first by using 10−20% gradient Tris-Glycerol SDS-PAGE (Lonza) to confirm the purity and molecular weight. The samples were prepared in loading buffer containing 0.1% SDS and heated for 5 min prior to loading on the gel at temperatures ranging from room temperature to 100 °C. The concentration of the proteins was quantified using UV absorption at 280 nm on a Biomate3 (Thermo Scientific). The extinction coefficient used to convert absorbance to concentration was calculated based on the tyrosine and tryptophan content of the peptides.[44] To observe the folding of the foldon domain, circular dichroism spectra were obtained using an Aviv 215 CD spectropolarimeter.

Transition temperatures of ELP solutions were determined by solution turbidity measured using a Cary 50 Bio UV−vis spectrophotometer equipped with a temperature-controlled cell (Varian). Spectra from 800 to 200 nm were obtained at 0.5 °C steps with an average temperature ramp of 1 °C/min. The transition temperature is defined as the temperature corresponding to the midpoint of the baseline and maximum absorbance (approximate maximum slope) of the 350 nm absorbance curve.

Particle size measurements were performed using 90 Plus particle size analyzer (Brookhaven Instruments), which is a fixed angle (90°) dynamic light scattering instrument equipped with Peltier temperature control. The samples were carefully filtered using a 0.22 μm filter prior to loading in 1 cm × 1 cm quartz cuvettes. The measurements were made in 2 min runs and repeated at least twice and were analyzed by BIC software (Brookhaven Instruments). The results are the mean diameter of multimodal size distribution (MSD), being calculated by the software based on the non-negatively constrained least-squares (NNLS) algorithm.

Results

ELP with and without foldon were successfully expressed and purified with yields between 50 and 100 mg/L of culture. The foldon sequence is expected to fold as a homotrimer, resulting in a three-armed star polypeptide (Figure 1). An SDS PAGE of the $(GVGVP)_{40}$-foldon illustrates the formation and stability of the trimer (Figure 2). Samples heated to different temperatures in loading buffer containing 0.1% SDS prior to loading on the gel resulted in different band patterns. Since the foldon domain is stable up to concentrations of 2% SDS,[40] the foldon domain in the sample which was not heated remained folded, and the construct was observed at about 60 kDa, 3 times the weight of a single polypeptide chain. By heating the sample at temperatures of 65 °C or above, the foldon domain was completely denatured, and the individual polypeptide chains are observed at 20 kDa. This temperature is about 10 °C lower than the reported stability of the foldon domain, which is reasonable considering the presence of SDS in the loading buffer which will destabilize it. At intermediate temperatures (e.g., 45 °C) partial unfolding is observed where bands appear at both 20 and 60 kDa. Circular dichroism spectra of the $(GVGVP)_{40}$-foldon constructs further

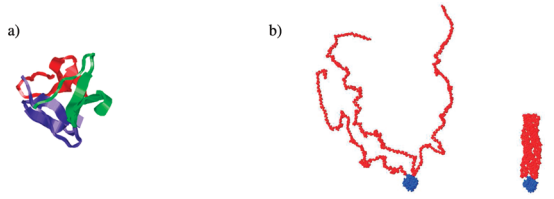

Figure 1. (a) Ribbon diagram of the foldon domain. This homotrimeric oligomerization domain is stable up to 70 °C in water (PDB accession number 1RFO).[39] Elastin-like polypeptide is added to the N-terminal residues to make the ELP trimer. (b) The three-armed star elastin-like polypeptide $(GVGVP)_{40}$-foldon before and after thermal transition. The foldon domain holds the three chains together below and above the ELP transition temperature. The contour length of the folded ELP reduces to about 20% of the unfolded one. The collapsed twisted filament ELP model[35] was created using Swiss PDB viewer based on reported backbone dihedral angles for the β-spiral structure.[34]

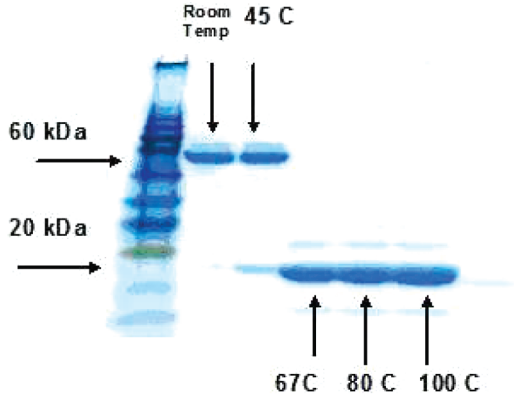

Figure 2. An SDS-PAGE gel of $(GVGVP)_{40}$-foldon with different degrees of heating prior to loading. The sample in lane 2 was not heated prior to loading on the gel, and it runs around 60 kDa, which is 3 times the size of a single $(GVGVP)_{40}$-foldon. The other lanes were heated for 5 min at the designated temperatures prior to loading on the gel. For the 45 °C sample, most of the polypeptide shows up as the trimer, but a small fraction of it runs as monomer (~20 kDa). The samples that were heated to temperatures above 65 °C resulted in the complete disruption of the trimers.

confirmed trimer formation by a peak at 228 nm which is characteristic of the folded foldon domain[38] (data not shown).

The defining characteristic of the environmental response of an ELP is the transition temperature (T_t), above which the protein solution becomes turbid, most frequently measured by absorbance in a UV−vis spectrometer. Representative data for obtaining the T_t of ELP and ELP-foldon constructs (Figure 3a) show a relatively sharp change in the 350 nm absorbance as a function of temperature for three different constructs. A linear relationship is observed between the T_t values of these ELP constructs and the logarithm of molar concentration of GVGVP pentapeptides (Figure 3b). Using the molar concentration of pentapeptide normalizes the samples to the total amount of ELP in solution. This represents an equivalent molar concentrations for the $(GVGVP)_{40}$-foldon trimer and linear $(GVGVP)_{120}$, whereas the $(GVGVP)_{40}$ is at 3 times the molar concentration of the others. Even at a higher molar concentration, the T_t of linear $(GVGVP)_{40}$ is higher than that of $(GVGVP)_{40}$-foldon. The transition temperature of ELP-foldon trimer is higher than a linear ELP with the same molecular mass, indicating that the molecular geometry affects the T_t. The similar slopes of the two samples indicate that the three-armed geometry results in a constant increase in T_t at equivalent concentrations.

The linear dependence of the transition temperature on salt concentration, a well-described phenomenon,[45,46] is observed for

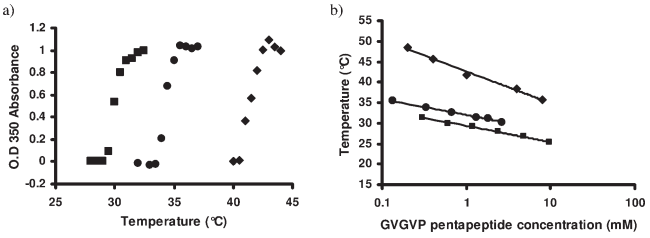

Figure 3. (a) Determination of the ELP and ELP-foldon transition temperatures. Transition temperatures are characterized for 25 μM solutions of $(GVGVP)_{40}$ (diamonds), $(GVGVP)_{40}$-foldon (circles), and $(GVGVP)_{120}$ (squares) in PBS by measuring UV absorbance at 350 nm as a function of temperature with a temperature ramp of 1 °C/min. The transition temperature is defined as the temperature at the midpoint between the baseline and maximum turbidity (approximately the steepest slope). For these samples, the transition temperatures are 41.5 °C for $(GVGVP)_{40}$, 34.5 °C for $(GVGVP)_{40}$-foldon, and 30.0 °C for $(GVGVP)_{120}$. (b) Transition temperatures of $(GVGVP)_{40}$ (diamonds), $(GVGVP)_{40}$-foldon (circles), and $(GVGVP)_{120}$ (squares) as a function of molar concentration of GVGVP pentapeptides (i.e., constant ELP mass concentration). A linear relationship between T_t and log C is observed for each construct. Comparing $(GVGVP)_{40}$-foldon and $(GVGVP)_{120}$, which have the same ELP molecular weight, the slopes are the same, but the former has higher T_t values.

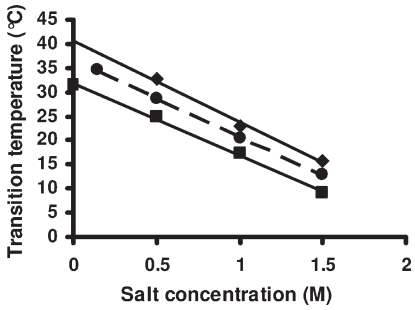

Figure 4. Effect of salt on the transition temperature of $(GVGVP)_{40}$ (diamonds), $(GVGVP)_{40}$-foldon (circles), and $(GVGVP)_{120}$ (squares). There is a linear relationship between salt concentration and the transition temperature of ELP-foldon solutions, except at low salt concentrations. At salt concentrations below 45 mM, a transition temperature is not observed by turbidity measurements. This contrasts the typical ELP, which exhibits transitions even without salt. The slopes for the three samples are equivalent, indicating that the geometry does not affect the salt dependency of the T_t for the ELP molecules. The $(GVGVP)_{40}$-foldon transition temperatures for all salt concentrations fall between $(GVGVP)_{40}$ and $(GVGVP)_{120}$.

the three-armed ELP. The transition temperature decreases linearly as a function of the sodium chloride concentration (Figure 4). This relationship suggests the zero salt concentration transition temperature for a $(GVGVP)_{40}$-foldon solution with 25 μM protein should be 38 °C. This is not observed. At salt concentrations below 50 mM, no turbidity is observed up to the temperature of the foldon stability (~70 °C), well above the expected transition temperature. Even when the solutions are held at these temperatures for extended times no phase separation is observed. This is in contrast to the linear $(GVGVP)_{40}$, which exhibits a T_t even at zero salt concentration. The near-identical slopes of the curves in this figure suggest that the effect of salt in decreasing the transition temperature is independent of geometry and molecular weight of the constructs.

Dynamic light scattering particle sizing was used to further investigate aggregation, particularly in low salt solutions (Figure 5). Below the transition temperature, the linear $(GVGVP)_{40}$ is soluble as observed by a polymer chain conformation size of less than 10 nm. Above the transition temperature, it aggregates into particles of about 500 nm in size. This particle formation is consistent with the turbidy observed for these

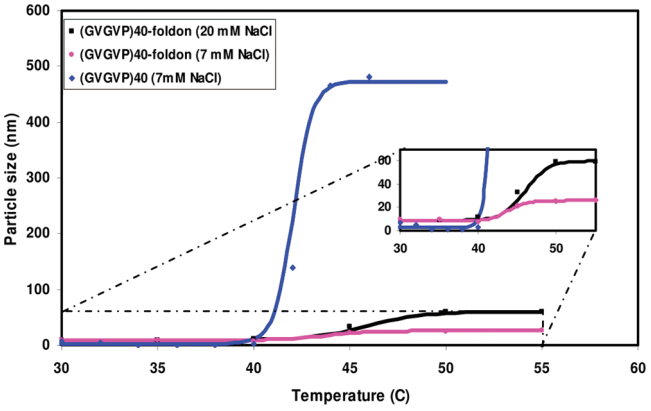

Figure 5. Dynamic light scattering particle size determination as a function of temperature for $(GVGVP)_{40}$ and $(GVGVP)_{40}$-foldon. The solutions are in low salt concentration and the graphs show very clear difference between the sizes of the particles above the transition temperature. For $(GVGVP)_{40}$ the particle size changes from below 10 nm to about 500 nm, resulting in turbidity of the solution. In the case of $(GVGVP)_{40}$-foldon, the diameter of particles does not exceed 30 nm when the salt concentration is 7 mM and 60 nm for a salt concentration of 20 mM. These solutions remain clear and the particle diameter does not change over time. This is also a reversible process as no difference in particle size as a function of temperature is observed when the sample is cooled. The inset is a magnification of the graph illustrating the region where small particles form.

solutions. For the $(GVGVP)_{40}$-foldon trimers, a distinctly different behavior is observed. At salt concentrations below 15 mM, when heated from below to above its expected transition temperature (based on the linear relationship to salt concentration), the size changes from below 10 nm to about 30 nm. The small aggregate size explains why no turbidity is observed by UV absorption under these conditions. For salt concentrations between 15 mM and about 45 mM, when the solution is heated to temperatures above the transition temperature, the size of the particles change to about 60 nm. The formation of the small particles at low salt is a reversible process as is observed by cooling down the solution and observing no hysteresis between warming and cooling experiments.

Further measurements demonstrate that the size of the aggregate is dependent on salt concentration, with three distinct regimes (Figure 6). In regime I, at salt concentration below 15 mM, the aggregates are 30 nm or smaller and appear to linearly increase with salt concentration. For salt concentrations between 15 and 45 mM (regime II), the size of the aggregates is approximately constant in the range of 60−65 nm, and in regime III, for salt concentrations above 45 mM, the particles are large and turbidity is observed which is consistent with the UV turbidity measurements. The particle size distributions in all three regimes are quite narrow having peak widths less than 1% of the particle diameters (Figure 6a).

The addition of SDS surfactant to the trimer solution generally led to a decrease in the stability of aggregates in both high and low salt conditions. SDS was added to two different $(GVGVP)_{40}$-foldon solutions with different salt concentrations. In one solution, SDS was changed from 0 to 0.05% while the salt concentration was kept constant at 7 mM (Figure 7). In this case, the particles were stable up to about 0.02% of SDS, and then the diameter of the particles dropped sharply in to what is expected to be a random coil polypeptide. In the case of the second solution with about 150 mM salt (Figure 7), the aggregates were not stable in the presence of SDS, and even at SDS concentration of 0.02% there was no turbidity.

Discussion

Typical ELP chains heated above their transition temperatures go from a random coil to a more ordered hydrophobic state and

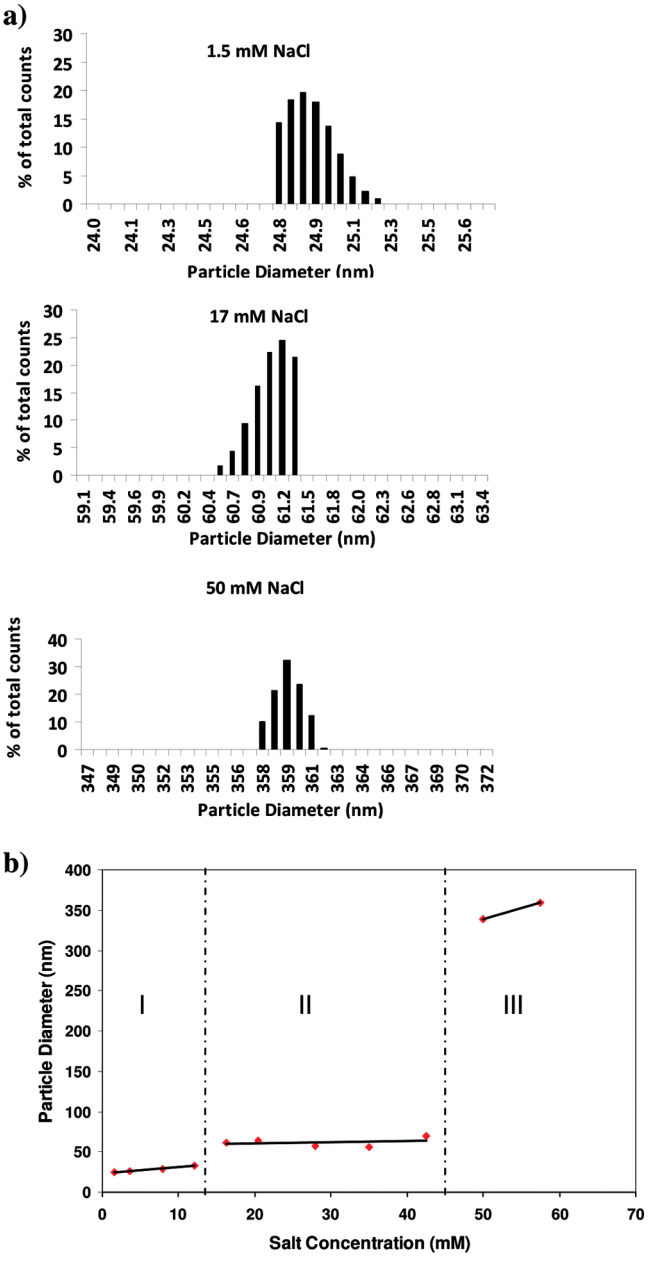

Figure 6. Dynamic light scattering of $(GVGVP)_{40}$-foldon in different NaCl concentrations. Dynamic light scattering was performed on 10 μM polypeptide solutions at 50 °C, which is above the polypeptide transition temperature. The measurements show very narrow distribution of particle sizes over a wide range of salt concentrations (a) and that the size of the aggregates varies as a function of salt concentration (b). Three zones are observed. For salt concentration below 15 mM, the particles are less than 30 nm and below. For salt concentrations between 15 and 45 mM the size of the particles are in the range of 60−65 nm. Increasing the salt concentration to values above 45 mM, the aggregates are greater than 300 nm and the solution becomes visibly turbid.

phase separate into a coacervate containing 63% water and 37% polypeptide.[1] Previous reports have shown that the initial formation of the coacervate phase is followed by aggregate growth and coalescence over time.[5,47] We would not expect significant differences in the behavior of the ELP when attached to the foldon domain, since aggregation above its transition temperature has been reported when ELP was used as a fusion protein for protein purification[43] and in the coiled-coil trimer of Fujita et al.[37] Like typical ELP, our data show that the three-armed ELP in moderate salt concentrations does exhibit a transition

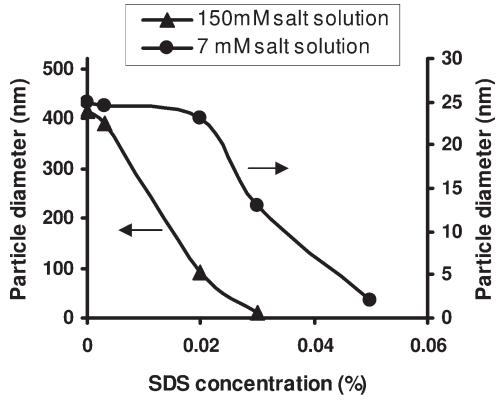

Figure 7. Effect of SDS on the $(GVGVP)_{40}$-foldon micelles and aggregates. At 150 mM salt (left axis), $(GVGVP)_{40}$-foldon aggregates of several hundred nanometers form above the transition temperature. SDS is able to disrupt the formation of these aggregates. SDS can also disrupt polypeptide micelle formation in low salt conditions (right axis) but requires higher concentrations.

temperature that is dependent on salt and ELP concentrations as well as an aggregate size that increases with time.

However, at low salt concentrations (<45 mM), the three-armed ELP, formed by ELP-foldon, behaves differently in comparison to linear ELP. Under these conditions, stable nanoscale aggregates form. Under further scrutiny, it is observed that there are two regimes of stable aggregates with considerably different size distributions (Figure 6b). We propose that each of these two regimes consists of stable micellar particles that do not coalesce over time, which is notably different from the higher salt regime. Below we interpret the size of these stable aggregates by considering the geometry of the ELP-foldon and the intermolecular interactions.

The foldon domain has a net negative charge and so can behave as a hydrophilic group to stabilize the coacervate aggregates formed by the ELP chains above their transition temperature. In essence, the ELP-foldon is a surfactant with three hydrophobic tails and a charged headgroup, which forms micelles at salt concentrations below 45 mM (regimes I and II). The salt concentration plays a key role in determining the size and type of aggregation that occurs in charged surfactant systems. The primary effect of salt in solution is to moderate the electrostatic interactions between charged species, however, salt can also modify hydrophobic interactions as is observed by the dependence of the transition temperature of ELPs on salt.

The geometry of any surfactant determines the size and shape of micellar aggregates,[48,49] based on the dimensionless packing factor:

$$v/a_0 l \tag{1}$$

where v and l are the volume and length of the hydrophobic tails, respectively, and a_0 is the effective area of the hydrophilic headgroup. If this dimensionless number is less than 1/3, spherical micelles will form with a size such that the diameter of the micelle will be

$$d = 6v/a_0 \tag{2}$$

For spherical micelles, the maximum diameter of the micelles is twice the length of the hydrophobic tail. Based on the ELP folding into a β-spiral and forming a triple strand,[1] the length of a $(GVGVP)_{40}$-foldon in its collapsed state is around 15 nm (Figure 1), corresponding to a maximum diameter of 30 nm for a spherical micelle. For $(GVGVP)_{40}$-foldon below its transition temperature, a micelle would have a maximum diameter of 150 nm. Based on the micelle size as a function of salt concentration, this indicates that regime I is consistent with spherical micelles with folded ELP chains. Regime II diameters are greater than 30 nm, which suggests that the micelles are either nonspherical or spherical micelles with unfolded or partially unfolded ELP chains.

We expect that the hydrophobic tails phase separate in the interior of the micelle into an immiscible coacervate-like phase, as in typical ELP solutions. Since the coacervate contains 37% protein and 63% water[1] and is slightly more dense than water, it is estimated that the volume occupied by the 120 pentapeptide repeats in a $(GVGVP)_{40}$-foldon trimer is $\sim$200 nm.[3] This is comparable with an estimation based on the molecular model of the collapsed ELP conformation occupying a cylinder of diameter 4.8 nm and length of 11 nm (Figure 1). Assuming a spherical micelle, this volume together with the micelle diameter can be used to calculate the headgroup areas. It is notable that regime I exhibits a slight increase in diameter with increasing salt. Based on eq 2, the apparent headgroup diameter is between 8 and 9 nm with a slight decrease as the salt concentration increases. Such a decrease in the headgroup size is not unexpected. The apparent area of the foldon domain, which has a net negative charge, will be affected by the electrostatic shielding of the additional salt.

In regime II, the micelle size remains approximately constant, corresponding to a headgroup diameter of about 5 nm if it were a spherical micelle. This value is slightly larger than the 2−3 nm diameter of the foldon domain, which suggests that they are not spherical micelles. Nevertheless, the constant size in this region suggests that the ion shielding is large enough that increasing the salt concentration does not result in any further reduction in headgroup area. This is consistent with a reduction in the Debye length to 2.5 nm at 15 mM NaCl. However, since the micelles are stable, the overall electrostatic interaction between micelles is apparently strong enough to prevent coalescence. As the salt concentration increases above 50 mM and we move into regime III, the charge on the foldon domains is shielded to a greater extent so that large aggregates will form.

The effect of increasing SDS concentration for both micellar and large aggregates of $(GVGVP)_{40}$-foldon results in a rather sharp decrease in the particles size, but the micellar aggregates show greater stability, since the large particles disaggregate at lower SDS concentration (Figure 7). These patterns give us criteria that can be used together with the salt dependency of the ELP-foldon micelles to predict the size of the aggregates. There is a limited range of salt and SDS concentration in which micelles can be made. The size of these particles for a $(GVGVP)_{40}$-foldon can be controlled and be kept as small as 20−30 nm. It is potentially possible to have even smaller micelles using shorter ELP chains.

Several other ELP micelles have been reported, most using a diblock polymer configuration. In recent work by Fujita et al. a hydrophobic block of different lengths of ELP was combined with a C-terminal hydrophilic polyaspartic acid block resulting in micellar particles.[24] They showed the formation of micelles only for ELP molecules with at least 80 pentapeptide repeats, and no micelle formation was observed for $(GVGVP)_{40}$. In another work by Dreher et al., two different ELP molecules with total length of 124−184 repeats of pentapeptide were used as the building block for micelle formation.[5] These two ELP molecules with two different transition temperatures were used to make micelles in the temperature range between their transition temperatures. These resulted in micelles of 35−45 nm.

Since our system uses a small hydrophilic headgroup, short ELP molecules can be used to make these micelles and quite small aggregates have been achieved. Additionally, the second hydrophilic block does not restrict the responsiveness of the micelles.

In a very recent study it has been shown that the transition temperature of block copolymers is also a function of the way that polarity is arranged and distributed along the ELP chain.[50] In an ELP block copolymer this can add to the complexity of controlling the transition temperature. For our system this is not an issue, and we are able to control the characteristics of the particles in a more precise way. This study demonstrates the possibility of making small micellar particles without the need of using block copolymers. Even though this approach relies on nonphysiological salt concentrations, there is no reason that modification of the headgroup cannot produce similarly small particles in physiologically applicable salt concentrations. This will make these particles appealing for applications such as targeted drug delivery.

Conclusions

We have designed and constructed a new responsive three-armed star elastin-like polypeptides and by using a trimer forming oligomerization domain. This new construct exhibits typical behavior of ELP molecules, except at low salt concentrations where it responsively forms micellar particles above its transition temperature. The process of micelle formation is thermally reversible and the particles are shown to be stable at temperatures above the transition temperature and can be made as small as 20−30 nm in diameter. The size of these micelles is among the smallest ELP particles that have been reported. Salt and surfactant were observed to affect the stability and size of the micelles, and by adjusting these two parameters the size of these particles can be controlled.

Acknowledgment. We thank X. L. Sun, Y. Ma, and the Department of Chemistry (CSU) for the use of equipment. This material is based upon work supported by the National Science Foundation (DMR-0908795) and a Faculty Research Development award from Cleveland State University.

References and Notes

(1) Urry, D. W. *J. Phys. Chem. B* **1997**, *101*, 11007.
(2) Urry, D. W.; Trapane, T. L.; McMichens, R. B.; Iqbal, M.; Harris, R. D.; Prasad, K. U. *Biopolymers* **1986**, *25*, S209.
(3) Urry, D. W.; Trapane, T. L.; Prasad, K. U. *Biopolymers* **1985**, *24*, 2345.
(4) Chen, W. Q.; Wei, H.; Li, S. L.; Feng, J.; Nie, J.; Zhang, X. Z.; Zhuo, R. X. *Polymer* **2008**, *49*, 3965.
(5) Dreher, M. R.; Simnick, A. J.; Fischer, K.; Smith, R. J.; Patel, A.; Schmidt, M.; Chilkoti, A. *J. Am. Chem. Soc.* **2008**, *130*, 687.
(6) Liu, H. Q.; Schmidt, J. J.; Bachand, G. D.; Rizk, S. S.; Looger, L. L.; Hellinga, H. W.; Montemagno, C. D. *Nat. Mater.* **2002**, *1*, 173.
(7) Maskarinec, S. A.; Tirrell, D. A. *Curr. Opin. Biotechnol.* **2005**, *16*, 422.
(8) Urry, D. W. *Trends Biotechnol.* **1999**, *17*, 249.
(9) Kasemo, B. *Surf. Sci.* **2002**, *500*, 656.
(10) Na, K.; Jung, J.; Kim, O.; Lee, J.; Lee, T. G.; Park, Y. H.; Hyun, J. *Langmuir* **2008**, *24*, 4917.
(11) Xu, F.; Joon, H. M.; Trabbic-Carlson, K.; Chilkoti, A.; Knoll, W. *Biointerphases* **2008**, *3*, 66.
(12) Nath, N.; Chilkoti, A. *Adv. Mater.* **2002**, *14*, 1243.
(13) Eddington, D. T.; Beebe, D. J. *Adv. Drug Delivery Rev.* **2004**, *56*, 199.
(14) Harmon, M. E.; Tang, M.; Frank, C. W. *Polymer* **2003**, *44*, 4547.
(15) Eichenbaum, G. M.; Kiser, P. F.; Simon, S. A.; Needham, D. *Macromolecules* **1998**, *31*, 5084.
(16) Valiaev, A.; Abu-Lail, N. I.; Lim, D. W.; Chilkoti, A.; Zauscher, S. *Langmuir* **2007**, *23*, 339.
(17) Alonso, M.; Reboto, V.; Guiscardo, L.; Mate, V.; Rodriguez-Cabello, J. C. *Macromolecules* **2001**, *34*, 8072.
(18) Strzegowski, L. A.; Martinez, M. B.; Gowda, D. C.; Urry, D. W.; Tirrell, D. A. *J. Am. Chem. Soc.* **1994**, *116*, 813.
(19) Chilkoti, A.; Dreher, M. R.; Meyer, D. E. *Adv. Drug Delivery Rev.* **2002**, *54*, 1093.
(20) Kopecek, J. *Biomaterials* **2007**, *28*, 5185.
(21) McGrath, K. P.; Fournier, M. J.; Mason, T. L.; Tirrell, D. A. *J. Am. Chem. Soc.* **1992**, *114*, 727.
(22) Nagapudi, K.; Brinkman, W. T.; Leisen, J.; Thomas, B. S.; Wright, E. R.; Haller, C.; Wu, X. Y.; Apkarian, R. P.; Conticello, V. P.; Chaikof, E. L. *Macromolecules* **2005**, *38*, 345.
(23) Osborne, J. L.; Farmer, R.; Woodhouse, K. A. *Acta Biomater.* **2008**, *4*, 49.
(24) Fujita, Y.; Mie, M.; Kobatake, E. *Biomaterials* **2009**, *30*, 3450.
(25) Adams, M. L.; Lavasanifar, A.; Kwon, G. S. *J. Pharm. Sci.* **2003**, *92*, 1343.
(26) Kataoka, K.; Harada, A.; Nagasaki, Y. *Adv. Drug Delivery Rev.* **2001**, *47*, 113.
(27) Meyer, D. E.; Chilkoti, A. *Biomacromolecules* **2002**, *3*, 357.
(28) Urry, D. W.; Parker, T. M.; Reid, M. C.; Gowda, D. C. *J. Bioact. Compat. Polym.* **1991**, *6*, 263.
(29) Megeed, Z.; Cappello, J.; Ghandehari, H. *Adv. Drug Delivery Rev.* **2002**, *54*, 1075.
(30) Herrero-Vanrell, R.; Rincon, A. C.; Alonso, M.; Reboto, V.; Molina-Martinez, I. T.; Rodriguez-Cabello, J. C. *J. Controlled Release* **2005**, *102*, 113.
(31) Betre, H.; Liu, W.; Zalutsky, M. R.; Chilkoti, A.; Kraus, V. B.; Setton, L. A. *J. Controlled Release* **2006**, *115*, 175.
(32) Brown, E. M. *Physiol. Rev.* **1991**, *71*, 371.
(33) Cardone, R. A.; Casavola, V.; Reshkin, S. J. *Nat. Rev. Cancer* **2005**, *5*, 786.
(34) Venkatachalam, C. M.; Urry, D. W. *Macromolecules* **1981**, *14*, 1225.
(35) Urry, D. W. *J. Protein Chem.* **1988**, *7*, 81.
(36) Yamaoka, T.; Tamura, T.; Seto, Y.; Tada, T.; Kunugi, S.; Tirrell, D. A. *Biomacromolecules* **2003**, *4*, 1680.
(37) Fujita, Y.; Funabashi, H.; Mie, M.; Kobatake, E. *Bioconjugate Chem.* **2007**, *18*, 1619.
(38) Frank, S.; Kammerer, R. A.; Mechling, D.; Schulthess, T.; Landwehr, R.; Bann, J.; Guo, Y.; Lustig, A.; Bachinger, H. P.; Engel, J. *J. Mol. Biol.* **2001**, *308*, 1081.
(39) Guthe, S.; Kapinos, L.; Moglich, A.; Meier, S.; Grzesiek, S.; Kiefhaber, T. *J. Mol. Biol.* **2004**, *337*, 905.
(40) Meier, S.; Guthe, S.; Kiefhaber, T.; Grzesiek, S. *J. Mol. Biol.* **2004**, *344*, 1051.
(41) Stetefeld, J.; Frank, S.; Jenny, M.; Schulthess, T.; Kammerer, R. A.; Boudko, S.; Landwehr, R.; Okuyama, K.; Engel, J. *Structure* **2003**, *11*, 339.
(42) Dong, H. J.; Nilsson, L.; Kurland, C. G. *J. Mol. Biol.* **1996**, *260*, 649.
(43) Meyer, D. E.; Chilkoti, A. *Nat. Biotechnol.* **1999**, *17*, 1112.
(44) Gill, S. C.; Vonhippel, P. H. *Anal. Biochem.* **1989**, *182*, 319.
(45) Cho, Y. H.; Zhang, Y. J.; Christensen, T.; Sagle, L. B.; Chilkoti, A.; Cremer, P. S. *J. Phys. Chem. B* **2008**, *112*, 13765.
(46) Reguera, J.; Urry, D. W.; Parker, T. M.; McPherson, D. T.; Rodriguez-Cabello, J. C. *Biomacromolecules* **2007**, *8*, 354.
(47) Cirulis, J. T.; Bellingham, C. M.; Davis, E. C.; Hubmacher, D.; Reinhardt, D. P.; Mecham, R. P.; Keeley, F. W. *Biochemistry* **2008**, *47*, 12601.
(48) Israelachvili, J.; Mitchell, J.; Ninham, B. *J. Chem. Soc., Faraday Trans. 2* **1976**, *72*, 1525.
(49) Lee, Y. S. *Self-Assembly and Nanotechnology: A Force Balance Approach*; Wiley-Blackwell: Oxford, 2008.
(50) Ribeiro, A.; Arias, F. J.; Reguera, J.; Alonso, M.; Rodriguez-Cabello, J. C. *Biophys. J.* **2009**, *97*, 312.